

**Kaon and pion emission in asymmetric C+Au and Au+C collisions at 1.0A GeV and 1.8A GeV**

A. Schmah,<sup>1</sup> S. Lang,<sup>1</sup> I. Böttcher,<sup>4</sup> F. Dohrmann,<sup>6</sup> A. Förster,<sup>1,\*</sup> E. Grosse,<sup>6,7</sup> P. Koczoń,<sup>2</sup> B. Koblmeier,<sup>4</sup> F. Laue,<sup>2,†</sup> M. Menzel,<sup>4</sup> L. Naumann,<sup>6</sup> H. Oeschler,<sup>1</sup> W. Scheinast,<sup>6</sup> T. Schuck,<sup>3,‡</sup> E. Schwab,<sup>2</sup> P. Senger,<sup>2</sup> Y. Shin,<sup>3</sup> H. Ströbele,<sup>3</sup> C. Sturm,<sup>1,2</sup> G. Surówka,<sup>2,5</sup> F. Uhlig,<sup>1</sup> A. Wagner,<sup>6</sup> and W. Walus<sup>5</sup>

(KaoS Collaboration)

<sup>1</sup>Technische Universität Darmstadt, D-64289 Darmstadt, Germany

<sup>2</sup>Gesellschaft für Schwerionenforschung, D-64220 Darmstadt, Germany

<sup>3</sup>Johann Wolfgang Goethe-Universität, D-60325 Frankfurt am Main, Germany

<sup>4</sup>Phillips Universität, D-35037 Marburg, Germany

<sup>5</sup>Jagiellonian University, PL-30059 Kraków, Poland

<sup>6</sup>Forschungszentrum Rossendorf, D-01314 Dresden, Germany

<sup>7</sup>Technische Universität Dresden, D-01062 Dresden, Germany

C. Fuchs, Amand Faessler, and H. Mansour

*Institute of Theoretical Physics, University of Tübingen, Auf der Morgenstelle 14, D-72076 Tübingen, Germany*

(Received 19 November 2004; published 30 June 2005)

The emission of  $K^+$  and  $\pi^\pm$  mesons has been studied in the asymmetric collision system Au+C and in the inverse reaction C+Au at 1.0A GeV (and at 1.8A GeV for C+Au only) in order to extract the effective source rapidities based on their distribution in the  $p_t$ - $y$  plane. The extracted source rapidity of  $K^+$  mesons is about  $y_s/y_{\text{beam}} = 0.25$  at both incident energies [ $y(\text{Au}) = 0$ ,  $y(\text{C}) = y_{\text{beam}}$ ]. This corresponds to a reaction volume consisting of the C nucleus and a tube cut out of the Au nucleus. In clear contrast, the source rapidities of  $\pi^\pm$  mesons vary from  $y_s/y_{\text{beam}} = 0.5$  in peripheral collisions (corresponding to  $NN$  interactions) to about  $y_s/y_{\text{beam}} < 0.33$  in central reactions. The multiplicities of  $K^+$  and  $\pi$  are compared to symmetric collision systems and, together with detailed transport model calculations, are used to study the sensitivity to the nuclear equation of state.

DOI: 10.1103/PhysRevC.71.064907

PACS number(s): 25.75.Dw

## I. INTRODUCTION

Pions and kaons emitted in heavy-ion collisions at beam energies close to their threshold in  $NN$  collisions serve as valuable probes of the dense nuclear matter produced in these reactions [1,2]. Especially,  $K^+$  mesons have turned out to be sensitive messengers of the high-density phase giving information on the stiffness of the nuclear equation of state [3,4].

Usually, symmetric collision systems have been studied as in this case, where the center of mass (c.m.) of the emitting system is well defined as being half of the beam rapidity. Consequently, spectra in the c.m. system, inverse slope parameters, and cross sections can be determined [3,5–9].

By using asymmetric collision systems (here, a C beam on a Au target and the inverse combination Au on C), the rapidity of the emitting source is *a priori* not known. It might vary between the rapidity corresponding to  $NN$  collisions ( $y_{\text{source}}/y_{\text{beam}} = 0.5$ ) and the one representing the complete amalgamation of the collision partners. On the other hand, the effective source rapidity can be extracted from the measured distribution of the emitted particles in space as done in this paper. A great

advantage is the use of one system in “normal” kinematics and the same one in “inverse” kinematics. In an earlier paper [10], only C on Au collisions had been studied. Other aspects in C+Au/Au+C collisions at the same incident energy have been investigated in [11,12].

The obtained source rapidity might be different for pions and kaons; it may vary with impact parameter and even with the momentum of the emitted particle. These results, which are only accessible using asymmetric collisions, offer new information on the underlying production mechanisms of the various particles. The source rapidity gives a measure of the effective size of the reaction volume and hence the number of nucleons involved in their production and emission. The extracted source rapidities are compared to estimates based on geometric concepts. Finally, yields, slope parameters, and multiplicities are compared to results obtained in symmetric systems. In view of extracting information on the compressibility of the nuclear matter from the yield of produced  $K^+$  [3,4], a comparison of C+Au and Ni+Ni collisions having similar numbers of participating nucleons turns out to be very interesting. It exhibits a different sensitivity to the stiffness parameter of the nuclear equation of state (EOS) as demonstrated along with model calculations.

## II. EXPERIMENT

The data were measured with the kaon spectrometer (KaoS) [13] at the SIS (Schwer-Ionen-Synchrotron) heavy-ion

\*Present address: CERN, CH-1211 Geneva 23, Switzerland.

†Present address: Brookhaven National Laboratory, Upton, NY, USA.

‡Present address: Max-Planck-Institut für Kernphysik, Heidelberg, Germany.

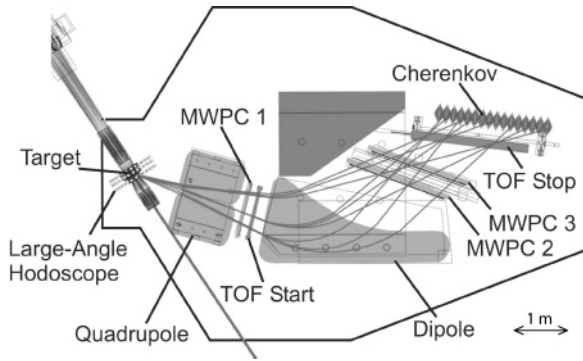


FIG. 1. Top view of the KaoS with its various components.

facility at the Gesellschaft für Schwerionenforschung (GSI) at Darmstadt. The experimental setup shown in Fig. 1 consists of a double-focusing quadrupole-dipole spectrometer, three multiwire-proportional-chambers (MWPCs 1 to 3), time-of-flight (TOF) start and stop walls, and one scintillator large-angle hodoscope (LAH) around the target point. The compact design of the spectrometer with particle flight paths of 5–6.5 m, a solid angle of up to 35 msr, and a momentum acceptance of  $p_{\max}/p_{\min} \simeq 2$  is matched to the requirements of kaon identification. The spectrometer can be moved around the target point from  $13^\circ$  to  $130^\circ$  with respect to the beam line. The two TOF walls serve as trigger of the data acquisition. Together with the target hodoscope they allow for two time-of-flight measurements. In combination with the reconstruction of the particle trajectories using the MWPCs (detection efficiency  $>95\%$ ) a strong background reduction is achieved making the detection of kaons possible at low incident energies. The Cherenkov detector array was not used in the present experiment. Figure 2 shows a mass distribution around the  $K^+$  mass after analysis. To extract the number of kaons, the remaining background is fitted with a polynomial and subtracted afterward. The “kaon peak” is integrated separately for various bins in  $p_{\text{lab}}$  with a width of  $3\sigma$ , which takes into account that the width of the mass spectra slightly increases with momentum.

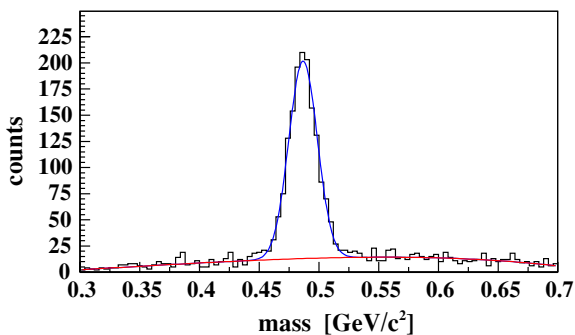


FIG. 2. (Color online) Mass distribution showing the  $K^+$  peak together with a Gaussian fit. The measurement refers to  $C \rightarrow Au$  at a beam energy of 1.8A GeV, a magnetic field setting of 0.6 T, and a polar angle of  $\Theta_{\text{lab}} = 44^\circ$ .

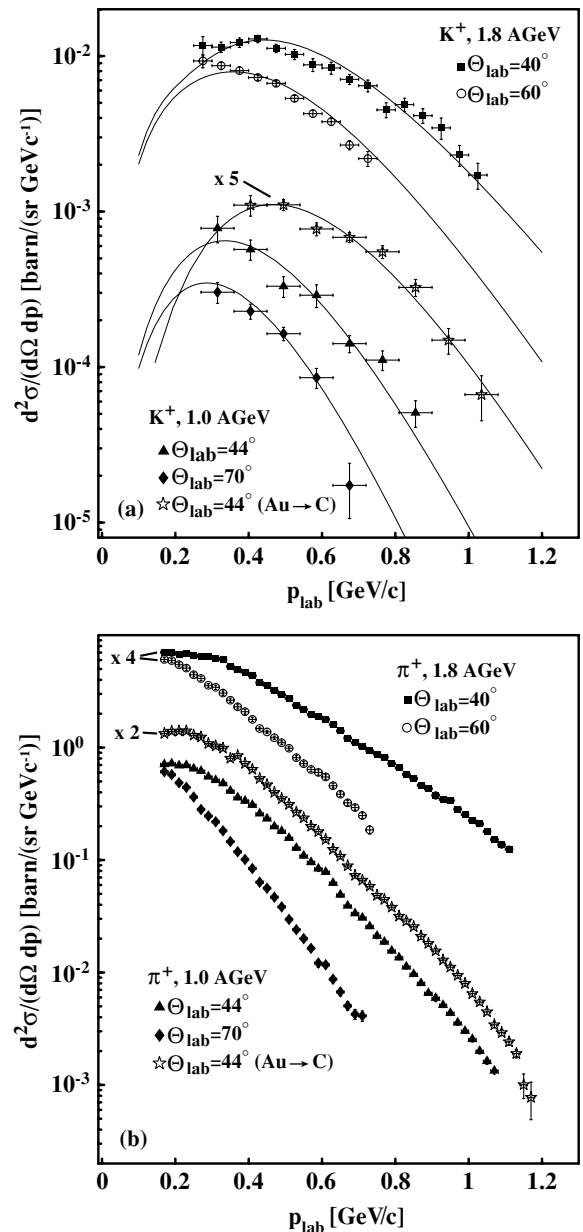


FIG. 3. Double differential cross sections of  $K^+$  mesons (a) and  $\pi^+$  (b) for inclusive collisions in the system  $C+Au/Au+C$  at 1.0A GeV as well as from  $C+Au$  at 1.8A GeV beam energy. The horizontal bars give the bin size. The thin lines in (a) show the calculated spectra using the parameters from the fits discussed later.

### III. EXPERIMENTAL RESULTS

The emitted  $K^+$  and  $\pi^\pm$  mesons in the colliding system  $C+Au$  at 1.0A and 1.8A GeV have been measured at laboratory angles  $\Theta_{\text{lab}} = 44^\circ, 70^\circ$  and  $\Theta_{\text{lab}} = 40^\circ, 60^\circ$ , respectively, and at  $\Theta_{\text{lab}} = 44^\circ$  in the inverse system  $Au+C$  at 1.0A GeV. A 1 mm Au target was used for the  $C+Au$  experiment, whereas a 5 mm C target was installed in the  $Au+C$  experiment. Figure 3 shows the measured double differential cross sections of  $K^+$  and  $\pi^+$  for inclusive reactions as a function of the laboratory momentum. The different slopes visible in these figures demonstrate the difference between the emission

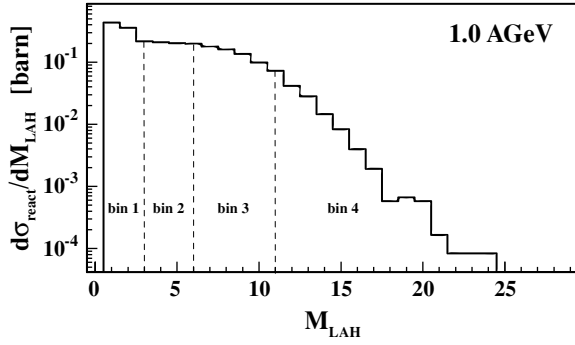


FIG. 4. Distribution of the measured multiplicity in the target hodoscope (LAH) at 1.0 A GeV for C+Au reactions together with the four chosen centrality classes.

system and the laboratory system, e.g., clearly visible for  $K^+$  at 1.0 A GeV at  $44^\circ$  for the two systems. The thin solid lines represent the results of the fits discussed later. They show the extrapolated range to low  $p_{\text{lab}}$  (used later for the integration) which amounts to 30–60%.

The multiplicity of charged particles in the target hodoscope (LAH) is proportional to the centrality of the collision. The corresponding distribution measured in the LAH has been divided into four centrality classes as shown in Fig. 4 for C+Au collisions at 1.0 A GeV. This is obtained for the minimum bias condition recorded independently of the particle trigger (TOF walls). Table I gives the chosen bins of the centrality classes together with the corresponding fraction of  $\sigma_{\text{react}}$ . The integral area of the spectrum represents the measured reaction cross section for C+Au reactions at 1.0 A GeV determined to  $\sigma_{\text{react}} = (2.6 \pm 0.3)$  b. Applying a geometrical model, one can calculate the impact parameter  $b$  using  $\langle b_j \rangle = \sqrt{\sigma_{\text{react}}^j / \pi}$  with  $\sigma_{\text{react}}^j$  calculated from the sum of fraction of  $\sigma_{\text{react}}$  beginning from central collisions up to the bin  $j$  under consideration. The results are shown in Table I.

#### IV. DATA ANALYSIS

The spectra are transformed into the Lorentz-invariant  $p_t$ - $y$  frame. The data of both experiments, C+Au and Au+C,

TABLE I. Selection of centrality classes for incident energies of 1.0 and 1.8 A GeV: Multiplicity range, fraction of the total cross section, and the corresponding impact parameters for each centrality class.

1.0 A GeV	Bin 1	Bin 2	Bin 3	Bin 4
Multiplicity	1–3	4–6	7–11	12–84
% $\sigma_{\text{react}}$	33.6	26.4	32.7	7.3
$\langle b_j \rangle$ (fm)	8.8	6.6	4.3	1.8
1.8 A GeV	Bin 1	Bin 2	Bin 3	Bin 4
Multiplicity	1–5	6–10	11–17	18–84
% $\sigma_{\text{react}}$	32.3	27.3	33.8	6.6
$\langle b_j \rangle$ (fm)	8.7	6.9	4.9	1.8

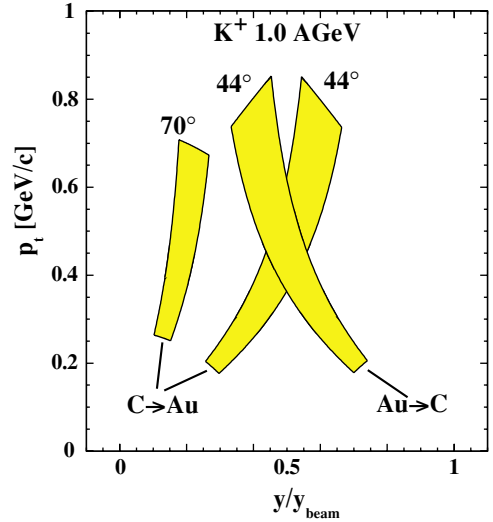


FIG. 5. (Color online) Phase-space coverage for  $K^+$  mesons at a beam energy of 1.0 A GeV. The marked areas refer to  $\Theta_{\text{lab}} = 44^\circ, 70^\circ$  for the system C+Au and to  $\Theta_{\text{lab}} = 44^\circ$  for the system Au+C [ $y(\text{Au}) = 0, y(\text{C}) = y_{\text{beam}}$ ].

are combined using the additive property of the rapidity by the transformation  $y_{\text{C+Au}} = y_{\text{beam}} - y_{\text{Au+C}}$ , and Fig. 5 shows measured phase-space coverage of  $K^+$  mesons at 1.0 A GeV.

Two different procedures are applied to extract the source rapidities. Method 1 uses a simple approach, while method 2 is more general.

#### A. Method 1

By transforming the spectra from the laboratory frame into various emitting source frames (center-of-mass systems) one can compare the total cross sections and inverse slope parameters of each transformation. In the correct source frame, the cross sections and inverse slope parameters  $T$  (if the spectra can be described with a Maxwell-Boltzmann distribution,  $\sigma^{\text{MB}} = CEe^{-E/T}$ ) of all spectra must be the same for a given incident energy. This is of course a rather simplified approach. An advantage of this method is an easy comparison of spectra from reactions of inverse kinematics as the transformation of the spectra leads to a clear crossing point when plotting cross sections and slope parameters  $T$  as a function of  $y_s/y_{\text{beam}}$  as can be seen in Fig. 6 for  $K^+$  mesons at 1.0 A GeV from C+Au and Au+C collisions. From the crossing region, a source rapidity of about  $y_s/y_{\text{beam}} = 0.25$  can be extracted. In this method, we assume an isotropic emission of all particles. This simple procedure works well only for  $K^+$  at 1.0 A GeV. The reason is (as will be shown next) that in this case the emission is indeed isotropic.

Pion spectra are usually described with two Boltzmann functions reflecting also a contribution from decaying  $\Delta$  resonances. The range setting for separating the two parts of each spectrum has unfortunately a strong influence on determining the crossing point of the temperatures and therefore of the source rapidity. For this reason, this method can only be applied for kaon spectra.

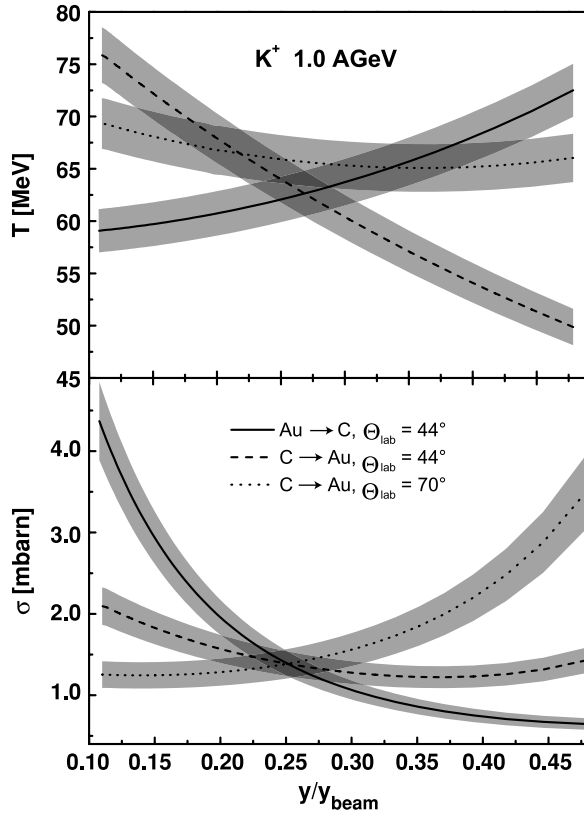


FIG. 6. Determination of the source velocity by transforming the spectra from the laboratory frame into emitting source systems with different  $y/y_{\text{beam}}$ . At the correct source rapidity  $y/y_{\text{beam}} = 0.25$ , both slopes and yields obtained at different angles and with both projectile-target combinations are expected to agree.

### B. Method 2

A more general method is based on a fit in the  $p_t$ - $y$  frame. An anisotropic emission from a source is the basis of the fit procedure. We compare the measured cross sections with lines of constant cross sections of the chosen particle-source

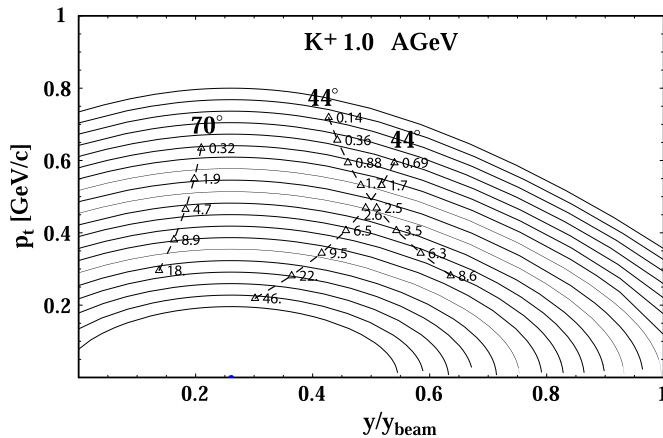


FIG. 7. Fit to spectra of  $K^+$  mesons at 1.0A GeV. Solid lines reflect constant values of invariant cross sections from a source rapidity at  $y_s/y_{\text{beam}} = 0.26 \pm 0.01$ . Emission in the polar angle is isotropic with  $a_2 = 0.0 \pm 0.4$ .

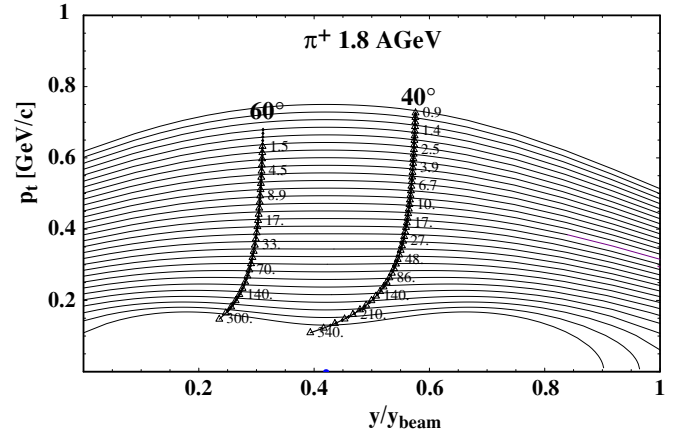


FIG. 8. Fit to spectra of semiperipheral (bin 2)  $\pi^+$  mesons at 1.8A GeV. The results of the fits are  $y_s/y_{\text{beam}} = 0.42 \pm 0.01$  and  $a_2 = 1.8 \pm 0.2$ .

distribution for  $K^+$  mesons at 1.0A GeV in Fig. 7 and of 1.8A GeV  $\pi^+$  mesons in Fig. 8. The measured values are shown by the symbols connected by dashed lines. The values are the measured cross sections. The solid lines represent the loci of constant cross sections from a source located at  $y_s/y_{\text{beam}}$  determined by a  $\chi^2$  procedure comparing the measured cross sections with the calculated values as will be explained next.

The parametrization of the invariant cross section  $\sigma^{\text{inv}}$  of a source with angular anisotropy has the form

$$\sigma^{\text{inv}} = [1 + a_2 \cos^2(\Theta_{\text{c.m.}})] \sigma^{\text{MB}}, \quad (1)$$

with  $\Theta_{\text{c.m.}}$  the polar emission angle of the particles in the c.m. system, and the factor  $a_2$  the strength of anisotropic emission in the polar angle. Only a symmetric function is used here, as an asymmetric contribution in the angular distribution cannot be distinguished from a change in rapidity.  $\sigma^{\text{MB}}$  is the invariant cross section parametrized by a Maxwell-Boltzmann distribution

$$\sigma^{\text{MB}} = EC e^{-\frac{E}{T}}. \quad (2)$$

With  $E = m_{\perp} c^2 \cosh(y - y_s)$  and  $m_{\perp} = \sqrt{(p_{\perp}/c)^2 + m^2}$ , we can write

$$\sigma^{\text{MB}} = \sqrt{p_{\perp}^2 c^2 + m^2 c^4} \cosh(y - y_s) C e^{-\frac{\sqrt{p_{\perp}^2 c^2 + m^2 c^4} \cosh(y - y_s)}{T}}. \quad (3)$$

Based on Eq. (3), a least  $\chi^2$ -fit routine was developed. The fit was divided into two steps. The first step determines the source rapidity and the  $a_2$  parameter. The second step fits the normalization factor  $C$  and the inverse slope parameter  $T$ . The separation into two independent steps is possible as only the shape of the distribution, not the absolute values of the cross sections, is necessary to determine the c.m. system. We compare the cross sections for the measured spectra along lines of constant cross section of the distribution with parameters  $a_2$  and  $y_s/y_{\text{beam}}$  within the range of measured  $p_t$ . Each spectrum with index  $i$  in Eq. (4) has crossing points with lines  $j$  of constant cross section. These points depend on the parameters

$a_2$  and  $y_s/y_{\text{beam}}$ . The resulting least  $\chi^2$  function

$$\chi^2 = \frac{1}{N} \sum_{j,i} \frac{|\hat{\sigma}_j^{\text{inv}}(y_s, a_2) - \sigma_{i,j}^{\text{inv}}(y_s, a_2)|^2}{|\Delta\sigma_{i,j}^{\text{inv}}(y_s, a_2)|^2} \quad (4)$$

is then only data based.  $\hat{\sigma}_j^{\text{inv}}$  is the average value of constant cross sections at line  $j$ .  $\sigma_{i,j}^{\text{inv}}(y_s, a_2)$  is a constant cross section of spectra  $i$  at the crossing point with line  $j$ .  $N$  is a normalization factor reflecting the number of crossing points. This method has the advantage that we have used only two fit parameters to find the c.m. system.

The errors of  $y_s/y_{\text{beam}}$  and  $a_2$  are determined from the  $\chi^2$  distribution in dependence of the two parameters  $y_s/y_{\text{beam}}$  and  $a_2$  at  $\chi_{\text{min}}^2 + 1$  [14].

For each chosen parameter set  $a_2$  and  $y_s/y_{\text{beam}}$  we fit the spectra with Eq. (1). The fit parameters  $C$  and  $T$  are in this method independent of  $a_2$  and  $y_s/y_{\text{beam}}$ . These values are determined within the range of measured  $p_t$ . To determine the total cross sections of the various particle species, Eq. (1) is integrated over  $p_t$  assuming a Maxwell-Boltzmann distribution which has been shown to describe the spectra in symmetric systems quite well [3,8]. Together with the integration in space, one obtains

$$\sigma = 4\pi \int_0^\infty \int_{y_s}^\infty [1 + a_2 \cos^2(\Theta_{\text{c.m.}})] EC e^{-\frac{E}{T}} p_t dy dp_t. \quad (5)$$

For pions, an expression composed of two Maxwell-Boltzmann distributions is used in order to take into account the contribution from decaying  $\Delta$  resonances as well (see, for example, [15]).

## V. RESULTS AND DISCUSSION

### A. Source rapidities

At both incident energies, inclusive  $K^+$  spectra and four centrality classes for pion spectra were analyzed. The results are summarized in Table II.

Figure 9 shows the extracted source rapidity  $y/y_{\text{beam}}$  for pions as a function of centrality. At peripheral collisions the source rapidities of pions reach the  $NN$ -limit ( $y_{\text{NN}}/y_{\text{beam}} = 0.5$ ). Pions need only an energy of 0.29 GeV/nucleon in the laboratory system to be produced and hence, they can easily be made in direct collisions. This explains the results for peripheral collisions. With increasing centrality the extracted source rapidities decrease. In central collisions there is more material of the target around the reaction zone and pions cannot escape easily. They might be absorbed and new pions might be created in secondary collisions. All these interactions occur predominantly with nucleons from the Au nucleus. Therefore, the resulting source rapidity is shifted towards target rapidity ( $y_{\text{Au}}/y_{\text{beam}} = 0$ ) in more central collisions. Within the error bars the  $\pi^+$  and  $\pi^-$ -source rapidities at 1.8A GeV are identical. The values obtained at 1.0A GeV are slightly higher (towards projectile rapidity).

The source rapidities of kaons (inclusive measurements) shown in the right part of Fig. 9 are about  $y_s^{K^+}/y_{\text{beam}} = 0.25$

TABLE II. Results of the extracted source rapidities  $y_s/y_{\text{beam}}$  and asymmetry parameters  $a_2$  with errors as explained in the text.

Particle	$E$ (A GeV)	Centrality	$a_2$	$y_s/y_{\text{beam}}$
$K^+$	1.0	Inclusive	$0.0_{-0.3}^{+0.5}$	$0.26_{-0.01}^{+0.01}$
$K^+$	1.8	Inclusive	$0.7_{-0.3}^{+0.2}$	$0.24_{-0.02}^{+0.01}$
$\pi^+$	1.0	Inclusive	$2.6_{-0.1}^{+0.2}$	$0.42_{-0.01}^{+0.01}$
$\pi^+$	1.0	Bin 1	$1.5_{-0.3}^{+0.2}$	$0.5_{-0.01}^{+0.01}$
$\pi^+$	1.0	Bin 2	$2.3_{-0.2}^{+0.3}$	$0.45_{-0.01}^{+0.01}$
$\pi^+$	1.0	Bin 3	$1.2_{-0.3}^{+0.1}$	$0.38_{-0.01}^{+0.01}$
$\pi^+$	1.0	Bin 4	$0.9_{-0.2}^{+0.1}$	$0.35_{-0.01}^{+0.01}$
$\pi^+$	1.8	Inclusive	$1.6_{-0.1}^{+0.2}$	$0.4_{-0.01}^{+0.01}$
$\pi^+$	1.8	Bin 1	$1.2_{-0.3}^{+0.1}$	$0.48_{-0.01}^{+0.01}$
$\pi^+$	1.8	Bin 2	$2.0_{-0.3}^{+0.3}$	$0.42_{-0.01}^{+0.01}$
$\pi^+$	1.8	Bin 3	$0.4_{-0.2}^{+0.1}$	$0.36_{-0.01}^{+0.01}$
$\pi^+$	1.8	Bin 4	$0.1_{-0.3}^{+0.1}$	$0.34_{-0.01}^{+0.01}$
$\pi^-$	1.8	Inclusive	$1.6_{-0.1}^{+0.2}$	$0.4_{-0.01}^{+0.01}$
$\pi^-$	1.8	Bin 1	$1.1_{-0.1}^{+0.2}$	$0.46_{-0.01}^{+0.01}$
$\pi^-$	1.8	Bin 2	$1.6_{-0.2}^{+0.2}$	$0.42_{-0.01}^{+0.01}$
$\pi^-$	1.8	Bin 3	$0.3_{-0.2}^{+0.2}$	$0.35_{-0.01}^{+0.01}$
$\pi^-$	1.8	Bin 4	$-0.1_{-0.1}^{+0.2}$	$0.34_{-0.01}^{+0.01}$

at both incident energies. This value is very different from those of the pions which are between  $y_s^{\pi^\pm}/y_{\text{beam}} = 0.35$  and 0.5. Kaons need at least 1.58 GeV in the laboratory system to be produced in  $NN$ -collisions. As expected, the results for kaons are far from the upper limit  $y_s/y_{\text{beam}} = 0.5$  for  $NN$ -collisions. The extracted source rapidity at 1.8A GeV is about equal to the one at 1.0A GeV. This indicates that at both incident energies the majority of kaons are produced in multi-step processes accumulating thereby the necessary energy to produce a  $K^+$ . As there are many more nucleons from the Au than from the C nucleus, additional interactions lead to a shift of the source rapidity away from  $NN$ -collisions towards the rapidity of the Au-nucleus.

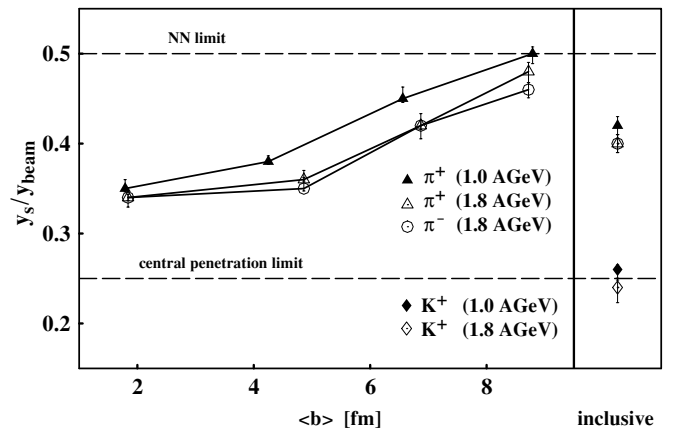


FIG. 9. Dependence of the extracted source rapidities on particle species for inclusive collisions (right side) and as a function of centrality (left side).

TABLE III. Cross sections and slope parameters of inclusive C+Au/Au+C collisions.

Particle	$E$ (A GeV)	$\sigma$ (b)	$T_1$ (MeV)	$T, T_2$ (MeV)
$K^+$	1.0	$(1.4 \pm 0.7) \times 10^{-3}$	—	$62 \pm 3$
$K^+$	1.8	$(40 \pm 10) \times 10^{-3}$	—	$82 \pm 2$
$\pi^+$	1.0	$2.1 \pm 0.1$	$46 \pm 3$	$68 \pm 2$
$\pi^+$	1.8	$5.3 \pm 0.9$	$47 \pm 3$	$90 \pm 2$
$\pi^-$	1.8	$6.9 \pm 1.1$	$39 \pm 2$	$86 \pm 2$

In a simple geometrical picture a limiting situation can be calculated. It corresponds to a central collision of a  $^{12}\text{C}$  nucleus drilling a tube into a Au nucleus (central penetration limit). In this case 12 nucleons from the carbon collide with 43 nucleons from the gold giving an  $A_{\text{part}}$  of 55. The corresponding source rapidity has a value of  $y_s/y_{\text{beam}} = 0.25$ . Indeed, the extracted values for  $K^+$  just correspond to this geometrical limit.

### B. Multiplicities and the nuclear equation of state

Having extracted the source rapidity and the asymmetry parameter of the angular distribution, we obtained the cross sections and inverse slope parameters by integration as described in the preceding section. The results for inclusive collisions are summarized in Table III. Knowing  $y_s$  and  $a_2$ , the laboratory spectra are converted into  $E_{\text{c.m.}}$  spectra as shown in Fig. 10 for  $K^+$  mesons. Identical spectra are obtained confirming the extracted parameters.

It is interesting to compare the results of this asymmetric collision system with symmetric ones. For this purpose, we

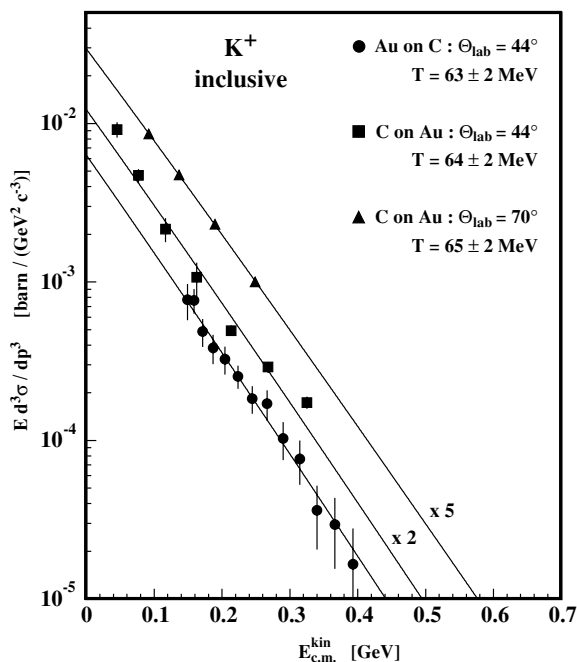


FIG. 10.  $E_{\text{c.m.}}$  spectra of  $K^+$  mesons from the colliding systems Au+C and C+Au at 1.0A GeV. The spectra are transformed to a system with the source rapidity of  $y_s/y_{\text{beam}} = 0.25$ .

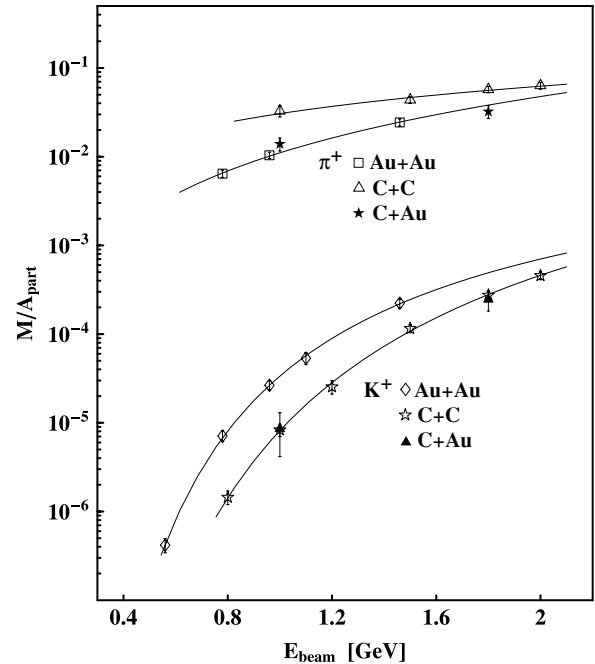


FIG. 11. Multiplicity per  $A_{\text{part}}$  for  $\pi^+$  and  $K^+$  as a function of the incident energy in comparison with inclusive collisions of the mass-symmetric systems C+C and Au+Au. The lines are drawn to guide the eye.

use the multiplicities per number of participating nucleons  $M/A_{\text{part}}$  to avoid a trivial size dependence. Multiplicities are obtained by dividing the cross sections from Table III by the geometrical reaction cross sections,  $\sigma_{\text{reac}} = 0.95$  b for C+C, 2.7 b for Ni+Ni, and 6.1 b for Au+Au. For symmetric collisions,  $A_{\text{part}}$  is set to  $A$  which takes into account that the  $K^+$  are predominantly produced in central collisions. For the asymmetric system C+Au, the rapidity of the  $K^+$ -emitting source has been established to  $y_s/y_{\text{beam}} = 0.25$ . In a strict sense,  $A_{\text{part}}$  is not yet defined by this value, but we have the ratio  $A_{\text{part}}(\text{proj})/A_{\text{part}}(\text{target})$ . In our example, we can set  $A_{\text{part}}(\text{proj})$  to 12, and we obtain  $A_{\text{part}} = 55$  which is used for  $K^+$ . From our analysis we found that  $A_{\text{part}}$  for pions is significantly lower. However, when comparing with symmetric systems, the corresponding values of  $A_{\text{part}}$  for pions are not available. For consistency and for simplicity, we have used for all reactions the same  $A_{\text{part}}$  as for  $K^+$ .

Figure 11 shows the results both for pions and for kaons as a function of the incident energy. The yield of pions in this representation is a factor of about 2 higher for the lightest system C+C than for Au+Au. This result can be interpreted as due to absorption in the larger system [3]. The asymmetric system C+Au is rather close to the value of Au+Au. In an analogous way, one can conclude that here also the yield is strongly influenced by absorption.

An opposite behavior is observed for the production of  $K^+$ : the yield in the heavy system Au+Au is five times higher than in the light C+C system. The underlying physics is the production mechanism via multiple collisions. They occur much more frequently in the heavy system which has reached higher density. The obtained multiplicities of the asymmetric

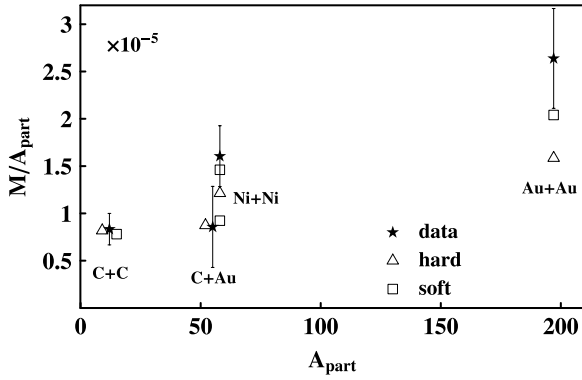


FIG. 12.  $A_{\text{part}}$  dependence of  $K^+$  multiplicities per  $A_{\text{part}}$  (inclusive collisions) at 1.0 A GeV. Data are shown as full star symbols. RQMD calculations using a soft ( $\kappa = 200$  MeV) and a stiff ( $\kappa = 380$  MeV) EOS are given as open symbols.

system happens to be closer to the light C+C system. One can interpret this as information on the number of secondary collisions which depends on the density reached in the system. The compression in C+Au will hardly exceed the values obtained in the C+C system.

The sensitivity of the  $K^+$  yield on the density has made these studies a key measurement for extracting information on the stiffness of nuclear matter. Indeed, the results shown in Fig. 11 have led to extraction of a stiffness parameter  $\kappa$  of around 200 MeV [3,4].

In this context, it is interesting to study the  $K^+$  multiplicity per  $A_{\text{part}}$  as a function of  $A_{\text{part}}$  at 1.0 A GeV incident energy together with model calculations from the Tübingen group. The transport calculations include a repulsive in-medium  $K^+N$  potential as proposed by effective chiral Lagrangians [16]. In this type of model the kaon-nucleon interaction consists of an attractive scalar part (Kaplan-Nelson term) and a repulsive vector part (Weinberg-Tomozawa term). The calculations are based on a  $K^+N$  potential that also accounts for in-medium modifications of the pion decay constant [17] leading to a repulsive net potential of  $\sim 30$  MeV at nuclear saturation density  $\rho_0 = 0.16 \text{ fm}^{-3}$ . Such an in-medium kaon potential is essential for reproducing the measured  $K^+$  yields as well as the kaon dynamics [4,18–20]. The nuclear mean field, on the other hand, is taken as a momentum-dependent Skyrme interaction using a stiff ( $\kappa = 380$  MeV) and a soft ( $\kappa = 200$  MeV) EOS. Details of the model can be found in [4,18].

Figure 12 shows the measured results as full stars. It appears already astonishing that Ni+Ni with a rather similar number of  $A_{\text{part}}$  has a higher yield than the asymmetric C+Au system. Furthermore, the sensitivity to the stiffness of the EOS extracted from relativistic quantum molecular dynamics (RQMD) calculations [18] is high for Ni+Ni and rather low for C+Au, as seen in Fig. 12. Also for C+C collisions, both assumptions give undistinguishable results. Thus, in both C+C and C+Au, no sensitivity to the stiffness of the nuclear equation of state is seen. For Ni+Ni and Au+Au collisions, in contrast, higher densities are reached, and a soft EOS gives yields that are about 30–40% higher than for a stiff EOS. The

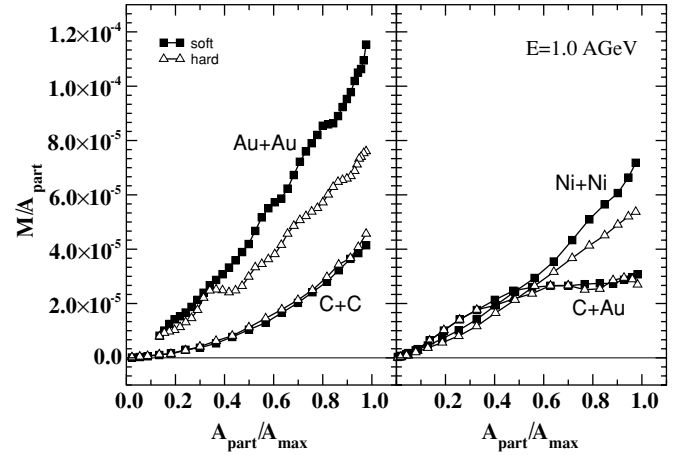


FIG. 13.  $A_{\text{part}}$  dependence of the  $K^+$  multiplicities in different mass systems obtained from transport calculations at 1.0 A GeV.  $A_{\text{part}}$  is normalized to the maximum number of participating nucleons, which is  $2A$  for symmetric systems and 55 for C+Au.

asymmetric system exhibits only an increase of about 10% for a soft compared to a hard EOS.

The difference between Ni+Ni and C+Au collisions becomes even more obvious considering the  $A_{\text{part}}$  dependence in exclusive reactions as predicted by the model calculations. A qualitative difference between C+C and C+Au on the one hand and Ni+Ni and Au+Au on the other can be seen from Fig. 13. In C+C and C+Au reactions, the  $K^+$  yield as a function of  $A_{\text{part}}$  is almost insensitive to the stiffness of the nuclear EOS. The Au+Au system, in contrast, shows a distinct EOS dependence. The enhanced kaon production caused by higher compression using a soft EOS becomes more pronounced with increasing centrality. The same effect occurs already in Ni+Ni.

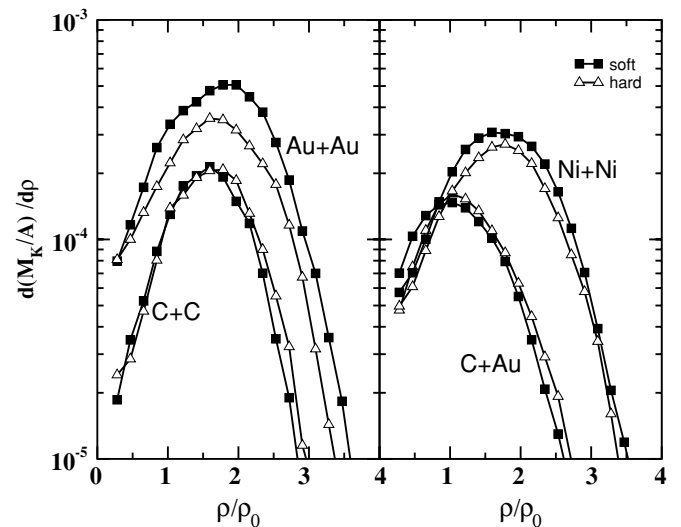


FIG. 14. Density distribution at the instant of  $K^+$  production calculated for the studied systems exhibiting values around normal nuclear matter density for C+Au while the other systems clearly have higher values.

The small sensitivity of C+Au to the nuclear EOS is because the densities hardly exceed normal nuclear matter values as can be seen in Fig. 14. Here the densities at the time of the  $K^+$  production are shown for the four systems studied. To explore the maximal effects, central reactions ( $b = 0$  fm) were chosen. Indeed, C+Au is centered around normal nuclear matter density, while the other systems are clearly grouped at higher values.

In C+Au a large fraction of kaons originates from the surrounding spectator matter of the Au nucleus. These particles are produced at normal nuclear density  $\rho_0$ , which explains the shift toward lower density values seen in Fig. 14. Hence, C+Au reactions show features that are otherwise typical for proton-nucleus reactions and explore the transition from  $p+A$  to  $A+A$ .

Both the measured  $K^+$  multiplicities and the model calculations exhibit a clear contrast between the results of C+Au and Ni+Ni in spite of similar values of  $A_{\text{part}}$ . This confirms the sensitivity of  $K^+$  production to density and hence to the stiffness of the EOS. Moreover, model calculations predict a linear dependence  $M \propto A_{\text{part}}$  in central C+Au which resembles that of pions and is distinct from the usually observed power law  $M \propto (A_{\text{part}})^\alpha$  [5]. Such a power law in symmetric systems is reproduced by transport models as well as by the statistical model when based on exact strangeness conservation [21]. Hence, the measurement of the  $A_{\text{part}}$  dependence in C+Au may help distinguish between the dynamical and the statistical approaches.

## VI. SUMMARY

For asymmetric collisions of C+Au and Au+C, the effective source rapidities for the emission of  $K^+$  and  $\pi^\pm$  are determined from the  $p_t$ - $y$  distribution by a fit procedure. The emitting source rapidities of kaons and pions turn out to be very

different. The kaons are emitted from a system moving with  $y_s^{K^+}/y_{\text{beam}} = 0.25$ , that corresponds to an emitting fireball consisting of a C nucleus amalgamated with a tube cut out of a Au nucleus. Pions in contrast are emitted from sources which vary from  $y_s^{\pi^\pm}/y_{\text{beam}} = 0.5$  for peripheral collisions (corresponding to  $NN$  collisions) to  $y_s^\pi/y_{\text{beam}} = 0.35$  for central collisions.

A comparison of the multiplicities per  $A_{\text{part}}$  of the asymmetric system C+Au with the symmetric reactions C+C and Au+Au shows that (i) the pion yield resembles Au+Au collisions and (ii) the kaons are closer to C+C interactions. This can be understood because the pion yield is strongly influenced by absorption and C+Au contains many nucleons able to absorb pions. The production of  $K^+$  below the  $NN$  threshold requires multiple interactions, and their rate depends strongly on the density reached. The densities reached in C+Au hardly exceed normal nuclear matter density, and hence their yield resembles the one of C+C. This reasoning is supported in detail by RQMD calculations showing the sensitivity of various quantities to the stiffness of the nuclear EOS. Comparing Ni+Ni and C+Au collisions as they have similar numbers of  $A_{\text{part}}$ , one observes a clear sensitivity to the stiffness of the EOS for Ni+Ni but not for C+Au. The measured multiplicity of  $K^+$  per  $A_{\text{part}}$  is higher for Ni+Ni than for C+Au. Indeed, Ni+Ni collisions reach higher densities than C+Au interactions. These studies confirm that the measurement of the  $K^+$  production in heavy-ion collisions is a sensitive tool for extracting the stiffness of the EOS.

## ACKNOWLEDGMENTS

This work was supported by the Bundesministerium für Bildung und Forschung (BMBF), by the Polish Committee of Scientific Research (No. 2P3B11515), and by the GSI fund for universities.

- 
- [1] C. M. Ko, Phys. Lett. **B138**, 361 (1984).
  - [2] J. Aichelin and C. M. Ko, Phys. Rev. Lett. **55**, 2661 (1985).
  - [3] C. Sturm *et al.* (KaoS Collaboration), Phys. Rev. Lett. **86**, 39 (2001).
  - [4] C. Fuchs, A. Faessler, E. Zabrodin, and Y.-M. Zheng, Phys. Rev. Lett. **86**, 1974 (2001).
  - [5] R. Barth *et al.* (KaoS Collaboration), Phys. Rev. Lett. **78**, 4007 (1997).
  - [6] F. Laue, C. Sturm *et al.* (KaoS Collaboration), Phys. Rev. Lett. **82**, 1640 (1999).
  - [7] P. Crochet *et al.* (FOPI Collaboration), Phys. Lett. **B486**, 6 (2000).
  - [8] M. Menzel *et al.* (KaoS Collaboration), Phys. Lett. **B495**, 26 (2000).
  - [9] K. Wisniewski *et al.* (FOPI Collaboration), Eur. Phys. J. A **9**, 515 (2000).
  - [10] F. Laue *et al.* (KaoS Collaboration), Eur. Phys. J. A **9**, 397 (2000).
  - [11] J. Lauret *et al.* (EOS Collaboration), Phys. Rev. C **57**, R1051 (1998); R. P. Scharenberg *et al.* (EOS Collaboration), *ibid.* **64**, 054602 (2001).
  - [12] K. Turzo *et al.* (Indra and Aladin Collaboration), Eur. Phys. J. A **21**, 293 (2004).
  - [13] P. Senger *et al.* (KaoS Collaboration), Nucl. Instrum. Methods A **327**, 393 (1993).
  - [14] P. R. Bevington and D. K. Robinson, *Data Reduction and Error Analysis* (McGraw-Hill, New York, 1992).
  - [15] C. Müntz *et al.* (KaoS Collaboration), Z. Phys. A **357**, 399 (1997).
  - [16] D. B. Kaplan and A. E. Nelson, Phys. Lett. **B175**, 57 (1986).
  - [17] G. E. Brown and M. Rho, Nucl. Phys. **A596**, 503 (1996).
  - [18] C. Fuchs *et al.*, Phys. Lett. **B434**, 245 (1998); Y.-M. Zheng *et al.*, Phys. Rev. C **69**, 034907 (2004).
  - [19] W. Cassing and E. L. Bratkovskaya, Phys. Rep. **308**, 65 (1999).
  - [20] Ch. Hartnack and J. Aichelin, J. Phys. G **27**, 571 (2001).
  - [21] J. Cleymans, H. Oeschler, and K. Redlich, Phys. Rev. C **59**, 1663 (1999); Phys. Lett. **B485**, 27 (2000).